Received: 22 February 2021 | Revised: 26 April 2021 | Accepted: 28 April 2021

DOI: 10.1002/nano.202100094

RESEARCH ARTICLE

Influence of TiC nano-particulates on the physical and mechanical properties of AA7150-TiC MMC: Fabricated by advanced novel process

Pagidi Madhukar[1] | **N. Selvaraj**[1] | **G.B. Veeresh Kumar**[2] | **C. S. P. Rao**[3] | **Faruq Mohammad**[4] | **R. Seetharam**[5] | **Murthy Chavali**[6]

[1] Department of Mechanical Engineering, National Institute of Technology-Warangal (NIT-W), Warangal, Telangana, India

[2] Department of Mechanical Engineering, National Institute of Technology-Andhra Pradesh (NIT-AP), Tadepalligudem, Andhra Pradesh, India

[3] National Institute of Technology-Andhra Pradesh (NIT-AP), Tadepalligudem, Andhra Pradesh, India

[4] College of Science, King Saud University, Riyadh, Kingdom of Saudi Arabia

[5] Department of Mechanical Engineering, PDPM Indian Institute of Information Technology, Jabalpur, Madhya Pradesh, India

[6] Department of Mechanical Engineering, NTRC-MCETRC and Aarshanano Composite Technologies Pvt. Ltd., Guntur District, Andhra Pradesh, India

Correspondence
Murthy Chavali, NTRC-MCETRC and Aarshanano Composite Technologies Pvt. Ltd., Guntur District, Andhra Pradesh, India.
Email: ChavaliM@gmail.com

Abstract

TiC_{np} reinforced AA7150 nanocomposites were prepared through a novel fabrication process (a combination of Vortex/Two-step Stir Casting/Ultrasonication). The effect of TiC_{np} (0.5, 1.0, 1.5, and 2.0 wt.%) and ultrasonication on both microstructure behavior as well as mechanical properties were investigated at room temperature. Microstructural studies were analyzed through optical and scanning electron microscopy for grain size refinement, nanoparticle distribution and failure analysis. Grain refinement and homogeneous distribution of nanoparticles were achieved due to the ultrasonication effect. The mechanical properties increase with the increase of TiC_{np} wt.%. The optimal peak value at 175 MPa in tensile strength, 177.05 HV in microhardness, and 41.07 μm in grain size reduction were achieved at 1.5 wt.% of TiC_{np} content, which was around 48.31% and 17.4% enhanced in strength, in microhardness and 52.37% in grain size reduction. These peculiar achievements resulted from the homogeneous dispersion of TiC nano-particulates in the nanocomposite material through a novel fabrication process.

KEYWORDS
AA7150, TiC, nanocomposites, mechanical properties, microstructures, ultrasonics

1 | INTRODUCTION

The development of any new product is mostly due to the advancement in the field of materials. Issues concerning the energy crisis have led to the necessity of lightweight alloys and metals in the transport industry have become so prominent. Aerospace and automobile industries have turned their focus toward composite material compared to aluminum (Al) and magnesium (Mg) alloys to improve fuel efficiency and have cleaner emissions. Though these are light-weight metals they do not meet the demand towards their material properties such as mechanical and tribological. A new kind of material called nanocomposite material was developed in which stiff ceramic particle are incorporated to get a notable improvement in properties[1–4] but low ductility and poor toughness limit the use of these materials, these being a result of poor wettability, low ductility, porosity, and clustering due to micro-nano particle sizes in nature.[5] Hence, several methods were introduced to minimize these defects.

Different processing methods are being used to fabricate metal matrix composites and these can be classified as semi-solid state, solid and liquid state fabrication process. In semi-solid-state, fabrication processes involve semi-solid forming,[6] compo-casting,[7] disintegrated melt deposition,[8] etc. In solid-state, fabrication processes involve spark plasma sintering,[9] powder metallurgy[10] and cold as well as hot working processes.[11] In the liquid state, fabrication processes involve pressure infiltration,[12] stir casting,[13] etc. Out of these fabrication techniques, stir casting is adopted due to its simplicity, most popular technique, and machine contains most economical as compared to other manufacturing processes.[14] The stir casting technique is also a convenient method for the mass production of sophisticated contour profiles as well as perfect for near-net profile processing. The stir casting method involves the blending of ceramic particles in molten liquid metal through a mechanical rotary stirrer[15–17] but the wettability causes severe problems during the mixing of nanoparticles into a molten bath and homogeneous distribution of nanoparticles.[18,19] In the real scenario, the quality of fabricated nanocomposites is affected by processing parameters like the viscosity of molten bath, the density of both matrix and ceramic reinforcements, stir casting parameters such as speed, blade angle and the pouring temperature of liquid metal etc. Most of the metal and molten alloys obey the Newtonium class of liquids with a range of viscosity from 10^{-3} to 10^{-2} Pascal-Second. In rotary mechanical stirring, the molten bath induces detrimental effects in its fluidity while incorporating ceramic reinforcement particles.[20] The main operation of the stirring process in the molten liquid is to disperse the reinforcement particle distribution throughout the melt and which can be attained in two ways: (a) stirrer creates turbulence towards the axial direction which generates the momentum to transfer particles from higher to lower zones and raise the particle and (b) create more shear effect which involves the breakup of agglomerations and distribution of particles in the radial direction to avoid the particles from sitting at crucible bottom during the stirring action.[14]

One of the main limitations of the mechanical rotary stirring technique to fabricate composite is to accomplish the homogeneous distribution of reinforcement particulates in metal liquid.[21] In this regard, we also noticed non-homogeneous dispersion[22] of reinforcement particulates in the composite material at a higher content. Ceramic nanoparticles create difficulties to attain uniform distribution of particulates during the production of nanocomposites due to poor wettability, high surface area-volume ratio. Vortex technique is adopted to incorporate the nanoparticles and avert the floating of nanoparticles as well as redirect them into molten bath. The optimal design (pure graphite stirrer with 30° blade angle, D/d (outer diameter of stirrer/inner diameter of crucible = 0.55) to produce vortex was proposed[23]; therefore, these issues promote the agglomerations/clusters of ceramic nanoparticles[24,25] which is very difficult to avoid but can be minimized by ultrasonic treatment. Ultrasonic vibration treatment distributes the particles from the agglomerations and restricts further cluster formation of ceramic nanoparticles which leads to uniform distribution.[26] A few researchers worked on ultrasonic vibration-assisted stir casting method to minimize the formation of clusters/agglomeration of ceramic nanoparticles[27–30] and achieved homogeneous distribution of nanoparticles throughout the composites as well as enhanced material properties. In this research work, a novel process has been developed and proposed to fabricate bulk nanocomposites with a homogeneous distribution of ceramic nanoparticles. Titanium Carbide (TiC) nanoparticles reinforced AA7150 nanocomposites were fabricated with a weight percentage of 0.5, 1.0, 1.5, and 2.0% TiC. The microstructure, particle distribution and mechanical properties were analyzed and correlated with the AA7150 base.

2 | MATERIALS AND METHODS

AA7150 was selected as base material due to its excellent "strength to weight ratio" as well as high corrosion resistance. It finds application in the lower and upper wings of aircraft. AA7150 was supplied by Venuka Enterprises, Hyderabad, India. TiC nanoparticles were supplied by platonic Pvt. Ltd., Jharkhand, with an average particle size (APS) of 30–50 nm, purity of > 99.5% and 4.93 g cc^{-1} density.

Ceramic TiC nanoparticles were chosen as reinforcement particles due to their excellent strength, hardness and wear properties to enhance the load-carrying capacity of an aircraft and wear resistance at the contact surface.

The advanced novel fabrication process and the effect of TiC nanoparticles on AA7150 were examined. EDS, XRD, SEM, OM were used to study the elemental composition, microstructure and particle distribution of monolithic and AA7150-TiC nanocomposites. Chemical composition of AA7150 alloy are Al: 87.3-90.3; Zn: 5.7-6.7; Cu: 1.2-1.9; Mg: 1.9-2.6; Si: ≤0.12; Cr: 0.10-0.22; Fe: ≤0.20; Mn: ≤0.20; Zr: 0.08-0.15 and the same confirmed with energy dispersive spectroscopy (EDS). The confirmation of materials through SEM, HRTEM and their elemental analysis of matrix and reinforcement particulates is shown in Figure 1.

The flow chart of the ultrasonic-assisted novel fabrication process is represented in Figure 2 and its detailed mechanism involved in each step of the advanced novel fabrication process as expressed in Figure 3.

Ultrasonic vibration-assisted stir casting setup was used to prepare nanocomposites and the setup consists of electrical resistance, ultrasonic probe, mechanical stirrer, ceramic crucible, ultrasonic control unit. The frequency of the ultrasonication probe was 20 KHz for producing Al-based nanocomposites of various weight percentages. Al alloy ingots were cut into small size pieces and were placed in the ceramic crucible having a capacity of 2 kg. The electrical furnace was heated to 750°C and the melt temperature was maintained for an hour to uniformly melt the liquid metal. The pellets were prepared by wounding Al foil TiC nanoparticles and the mold was preheated to 500°C and this was maintained for 30 minutes. The mechanical rotary stirrer was located in a liquid Al alloy and a vortex was created with the help of the stirrer at 350 rpm speed. The stirrer is made of stainless steel and coated with zirconium oxide to restrict the migration of ferrous ions from the stirrer material to the alloy melt while agitation is in progress. The system was also supplied Argon gas to avoid the formation of metallic oxides during the mechanical mixing process. Degassing table (hexachloroethane, C_2Cl_6) and Mg flex were slowly added to avoid gasses from the melt as well as to improve the wettability of nanoparticles in the molten liquid metal.

Preheated TiC nanoparticles were introduced in the vortex of molten liquid and thoroughly stirred until the particles were directed into molten liquid. Two-step mechanical stirring was performed for 20 minutes and each step engaged with 10 minutes of the stirring process. The induction power supply was lowered and the melt was allowed to reach a semisolid state at 550°C-600°C and then again it was heated to 750°C. Ultrasonication technique was introduced which contained titanium alloy probe of 20 mm diameter and 110 mm length dipped into the molten metal to about two-thirds of liquid alloy melt, for ultrasonic waves to pass and break nanoparticles clusters. During the ultrasonic vibration process, high-intensity energy waves were generated and passed through a molten liquid and when the energy went beyond the bonding energy of AA7150 alloy, these waves broke up the liquid metal bonds and created lots of cavitation bubbles throughout the liquid metal.

Due to high pressure and high-temperature differences, the cavities explode and disperse the nanoparticles indiscriminately due to acoustic streaming. Hence, the tendency of TiC ceramic nanoparticles agglomeration minimized significantly with a combined sequence of the vortex, two-step stir casting and effective ultrasonic vibration treatment (cavitation as well as acoustic streaming). Then ceramic crucible was separated from the electric furnace and molten composite was poured into the preheated (500 °C) mild steel die and allowed to solidify at room temperature.

All fabricated samples were used to examine the microhardness and tensile properties. "ECONOMET VH 1MD" (Chennai Metco Pvt. Ltd., Chennai, India; http://www.chennaimetco.com) apparatus was used for microhardness test and UTM (Instron with 10 kN load cell) was used for testing tensile properties of various samples. For microstructure and grain refinement studies, polished samples were analyzed with "QUASMO, QX-4RT" optical microscopy, SEM (Model No.: Vega-3 LMU, Tescan Analytics-Tescan Orsay Holding, Brno-Kohoutovice, Czech Republic; https://www.tescan-analytics.com/) for studying particle dispersion and fracture surface, EDS (Model No.: Ultim Max, Oxford Instruments, UK; https://nano.oxinst.com/) was used for the elemental analysis of monolithic and nanocomposite materials.

3 | RESULTS AND DISCUSSIONS

3.1 | Microstructure characterization of AA7150-TiC nanocomposites

The microstructure characterization of nanocomposites was examined through optical microscopy (OM), SEM to analyze the grain refinement, particle distribution and fracture surface analysis. OM photographs for ceramic TiC nanoparticle reinforced AA7150 alloy composites and unreinforced alloy material were shown at 50 μm in Figure 4A-E and followed by average grain size (AGS) graphical representation. It is calculated from the Linear Intercept Method and the maximum reduction is 41 μm. SEM micrographs for TiC nanoparticle reinforced nanocomposites to study the particle distribution and the

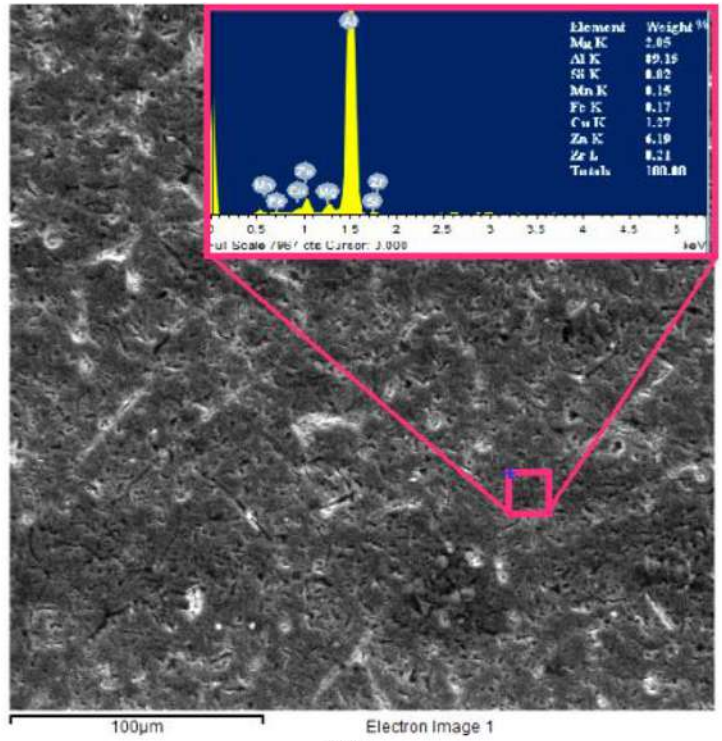

(A)

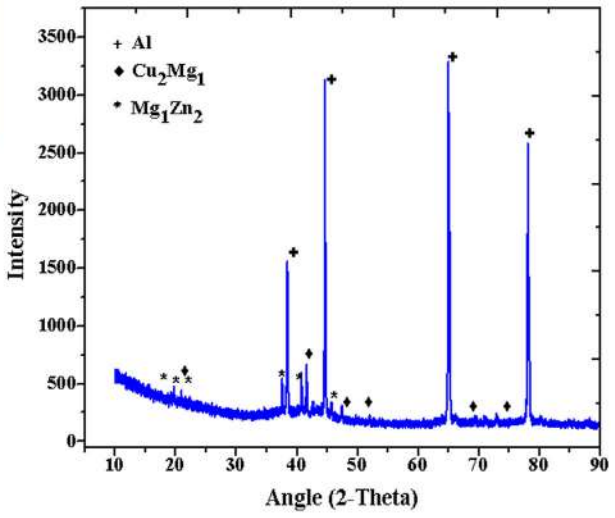

(B)

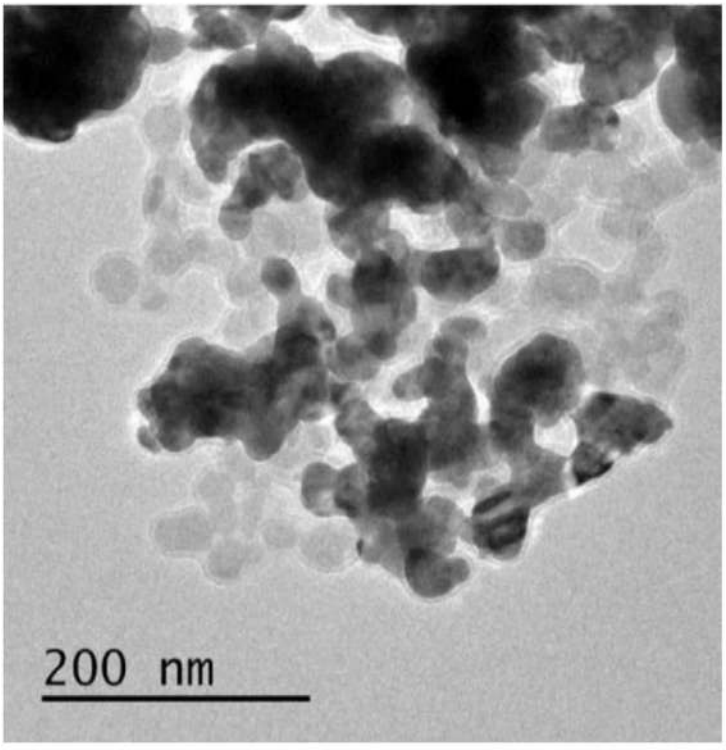

(C)

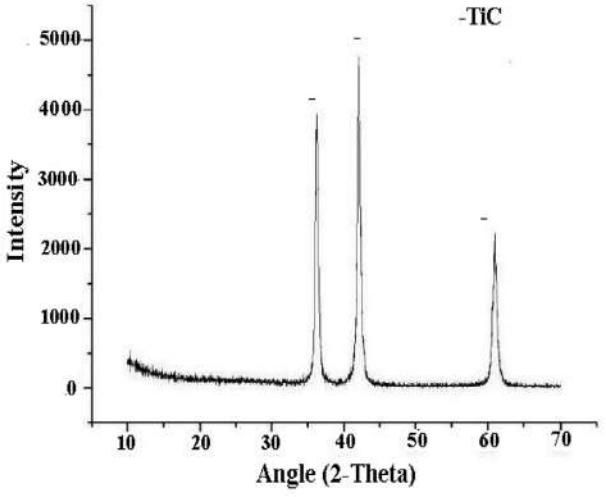

(D)

FIGURE 1 Material characterization of (A) AA7150 and its EDS spectrum for chemical composition (B) XRD spectrum of AA7150 (C) HRTEM of TiC manoparticles size at 200 nm (D) XRD pattern of TiC nanoparticles

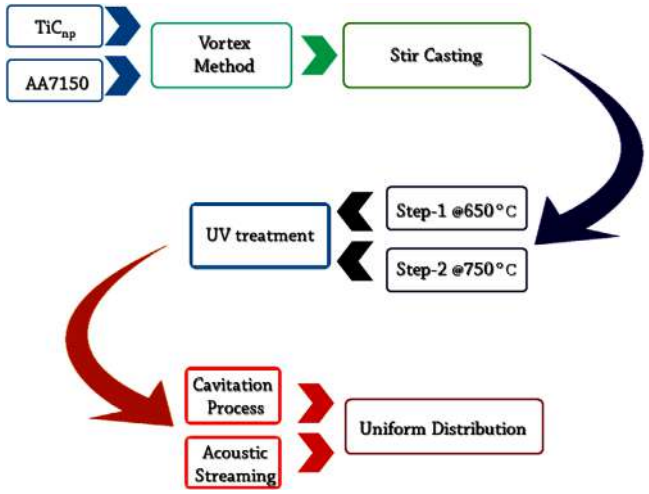

FIGURE 2 Flow chart of the advanced novel process

phenomenon was discussed in detail in Figure 3. EDS for elemental characterization of each nanocomposite and its nanoparticle size distribution graphs are shown in Figure 5 and also investigated the fracture surface for nature of failure analysis of nanocomposites.

At first, microstructural examinations were done on the prepared sample of monolithic and TiC nanoparticles reinforced nanocomposites and the grain boundary images are shown in Figure 4A-E. It is noticed that fair grain boundary structures were appearing due to the reinforcement of TiC nanoparticles. The majority of nanoparticles were repelled at the grain boundary areas and beyond 1.5 wt.%, TiC nanoparticles reinforcement formed the cluster or agglomerations and those were trapped between the grain boundaries. Also, observed that grain size reduces with the increase of wt.% of TiC nanoparticles reinforcement due to the ultrasonic effect (uniform dispersion of nanoparticulates through acoustic streaming, inter-particle distance and interfacial area analysis supported by Figure 5 SEM and histogram). During the ultrasonic vibration treatment in molten liquid, the grain size of primary α-Al decreases and the number of grains (α-Al) in composite material increases due to acoustic streaming and cavitation of UV treatment which leads to a homogeneous distribution of nanoparticles.[31,32] The AGS of the unreinforced and untreated composite is 86.23 μm and this reduces continuously by adding TiC nanoparticles reinforcement due to the ultrasonic effect. Secondly, the grain refinement of nanocomposites is strengthened because of the ultrasonic effect. This reduction of grain size leads to improvement in the strength of AA7150-TiC nanocomposites according to Hall-Petch theory.

Compared to other existing strengthening mechanisms, the grain refinement mechanism[33] is an attractive theory because it affects neither the toughness nor ductility of the materials. It was also proposed to explain that the fabrication process is capable of grain refinement with TiC nanoparticles reinforcement. The grain size of each composite was determined through a linear intercept method, a technique used to quantify the grain or crystal size for a given material by drawing a set of randomly positioned line segments on the micrograph, counting the number of times each line segment intersects a grain boundary and finding the ratio of intercepts to line length (i.e., AGS = length of line/number of intercepts). Line length was estimated through "ImageJ Software". From Figure 4F, it is noticed that the maximum grain size reduction at 1.5% TiC (41.07 μm) is 52.37% as compared to the base alloy matrix (86.23 μm).

SEM images of nanocomposites are (reinforced composites for nanoparticle distribution and respective histogram for nanoparticles size distribution) shown in Figure 5. It reveals the presence of TiC nanoparticles in AA7150 alloy and uniform distribution of nanoparticles in 0.5%, 1.0%, and 1.5 wt.% TiC except for 2 wt.% TiC. Therefore, an improvement in mechanical properties was observed due to the uniform distribution of particles as per Orowan strengthening theory but in 2 wt.% TiC, SEM micrograph reveal the formation of cluster or agglomeration. Figure 5 confirms the uniform distribution of TiC nanoparticles. The corresponding elemental analysis was studied through the EDS of each particle distribution photograph. EDS spectroscopy reveals a major element of AA7150 and TiC nanoparticle reinforcement with elemental peak intensities. It is also observed that the porosity of nanocomposites decreases with the increase of wt.% of TiC nanoparticles which plays a crucial influence in improving the properties of composites.

Minimum porosity and maximum TiC nanoparticle distribution were noticed at AA7150-1.5 wt.% of TiC nanocomposite (Figure 5C). The reduction of porosity and homogeneous dispersion of nanoparticles is mainly due to ultrasonic treatment which involves cavitation as well as acoustic streaming. This effect leads to the optimal strength of the nanocomposites according to the Orowan strengthening mechanism. The histogram representation for nanoparticle size distribution also supports uniform distribution of TiC nanoparticles which increases with the increase of ceramic nanoparticles wt.% by up to 1.5% TiC.

The majority of nanoparticles are dispersed (0-150 nm range) throughout the composite material due to the sonication effect and it is confirmed with histogram representation (Figure 5). The ImageJ software was used to find the size of nano-particulates and their distribution analysis in the nanocomposite material.[32] Figure 5C histogram shows more nanoparticles dispersed in the range of 30–120 nm compared to counterparts. Further improvement of nanoparticles (2% TiC) shows fewer particles

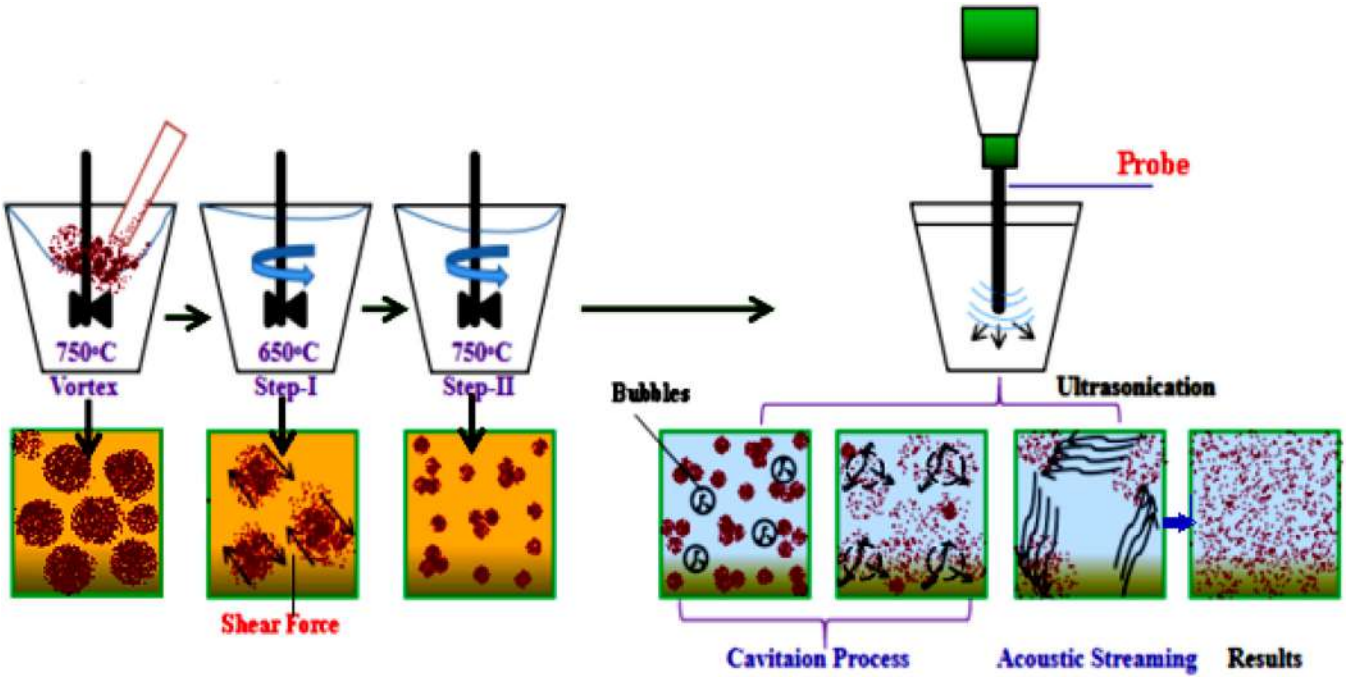

FIGURE 3 The mechanism of the novel fabrication process

distribution < 200 nm and more clusters or agglomerations in the range of 200–600 nm.

3.2 | Physical and mechanical properties of ultrasonic-assisted AA7150-TiC nanocomposites

To investigate the strengthening effect of TiC ceramic nanoparticles, the mechanical behavior of AA7150-TiC nanocomposites at room temperature were examined. AA7150 alloy and TiC nanoparticles have densities of 2.83 and 4.93 g cc^{-1}. In order to find the level of porosity in the fabricated samples, the experimental density and theoretical density of samples were calculated and are represented in Figure 6A.

The experimental density of various nanocomposite samples and monolith material was calculated through Archimedes' principle. Digital electron weighing balance was used to find the weight of the sample in air and distilled water. The theoretical densities of the various samples were evaluated through the rule of mixing formula. With the help of experimental and theoretical densities, the porosity of monolithic and nanocomposites which are reinforced with TiC nanoparticles of 0.5%, 1.0%, 1.5%, and 2.0% of weight at the as-cast state was calculated.

The porosity variation with wt.% of TiC reinforced nanocomposites is shown in Figure 6B. It is noticed that the porosity of nanocomposite decreases with the increase in weight percentages of nanoparticulate reinforcement.[30,34] It is due to the effect of ultrasonic waves which enhance the wetting of molten AA7150 alloy. TiC nanoparticles behave as nucleates to refine the grains of the matrix material. It is also observed that the % porosity reduction at 1.5 wt.% TiC is 69.87% and this can be attributed to the ultrasonic degassing effect of liquid metal, enhancement of fluidity by the uniform distribution of nanoparticles and ultrasonic vibration effect on liquid homogenization.[35,36]

Hardness test was carried out on Vickers microhardness tester at a load of 200 g and the 15 seconds of dwell period. Specimens were subjected to the indentation at various locations and an average of five readings was taken. The microhardness values of AA7150 and AA7150-TiC nanocomposites are graphically represented in Figure 7. The test results of Vickers hardness value with TiC reinforced nanocomposites were higher than the unreinforced matrix alloy. It is noticed that the inclusion of ceramic TiC nanoparticles to the AA7150 alloy matrix significantly increased the microhardness of nanocomposite material. It is confirmed (Figure 7) that the microhardness value of the nanocomposite material was enhanced with enhancement in ceramic nanoparticles wt.%. It also reveals that hardness increases up to 1.5 wt.% but it decreases on a further increase of TiC nanoparticles.

The optimal magnitude value of microhardness for AA7150-TiC nanocomposites which has 1.5 wt.% of TiC ceramic nanoparticles is 177.05 HV because of the existence of hard phase TiC nanoparticles, "Hall-Petch" and "Orowan strengthening mechanism", as well as uniform

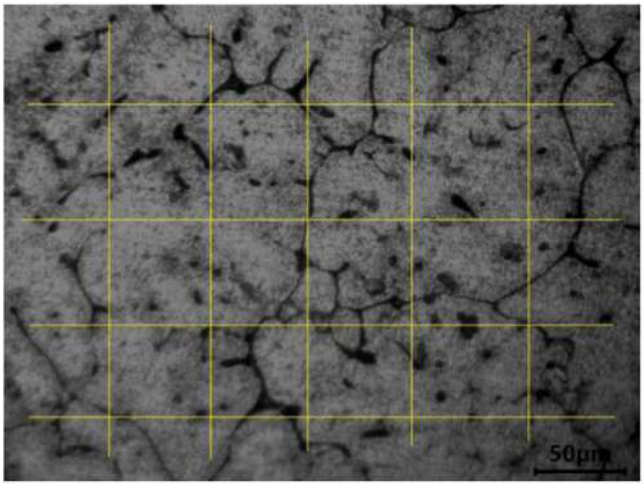

(A)

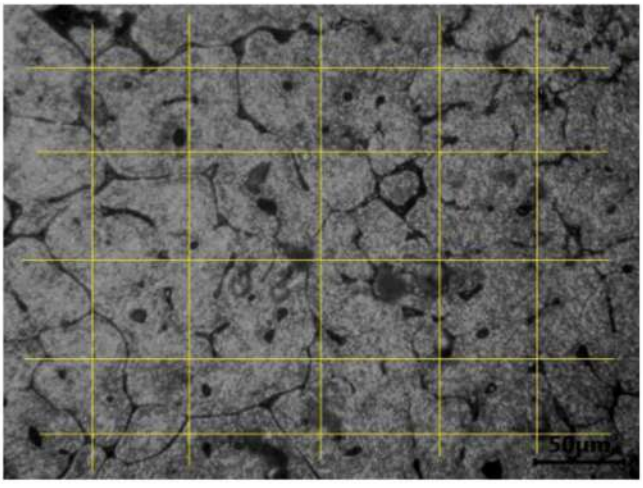

(B)

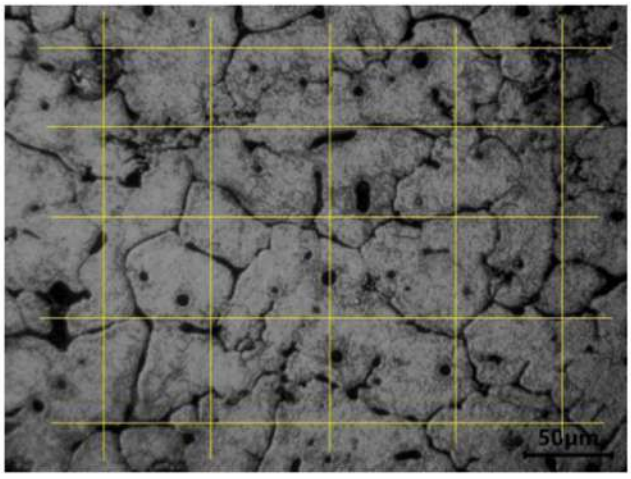

(C)

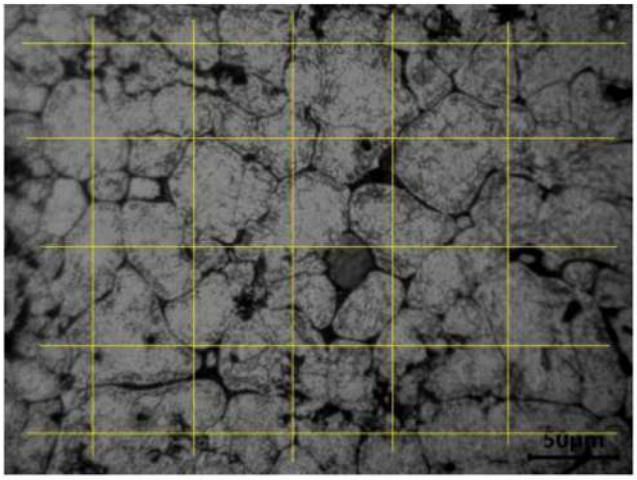

(D)

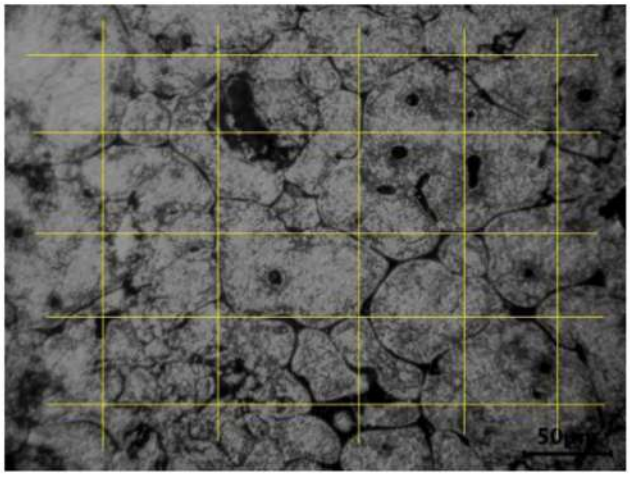

(E)

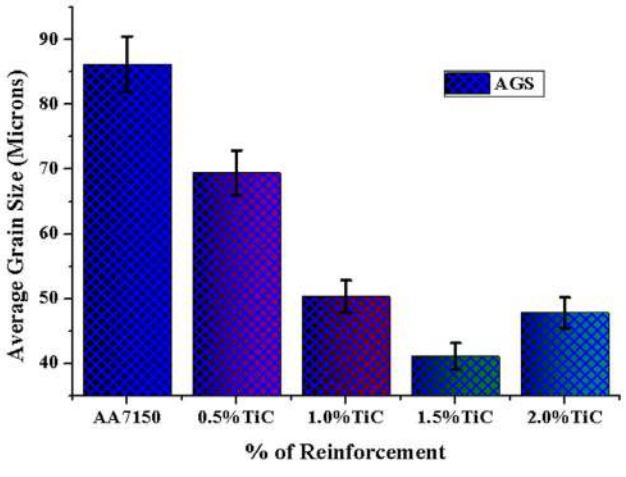

(F)

FIGURE 4 Optical microstructure of (A) AA7150 (B) AA7150-0.5% TiC (C) AA7150-1.0% TiC (D) AA7150-1.5% TiC (E) AA7150-2.0% TiC (F) AGS of each nanocomposite and alloy matrix

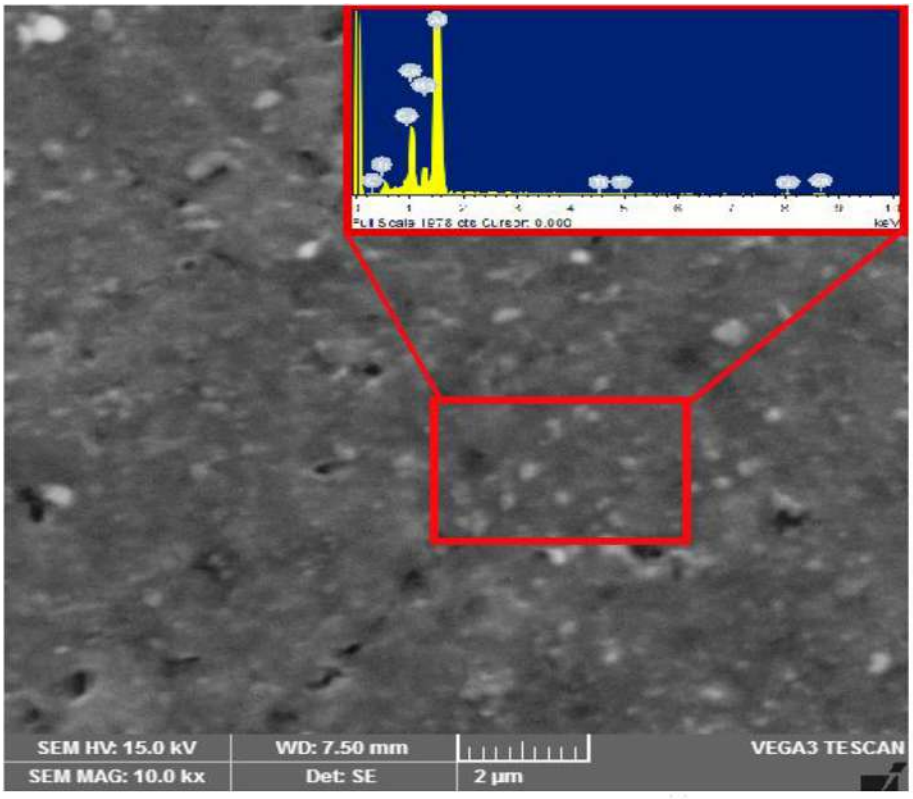

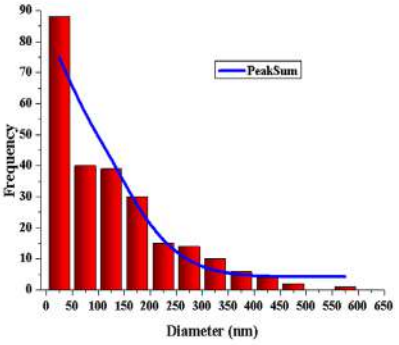

(A)

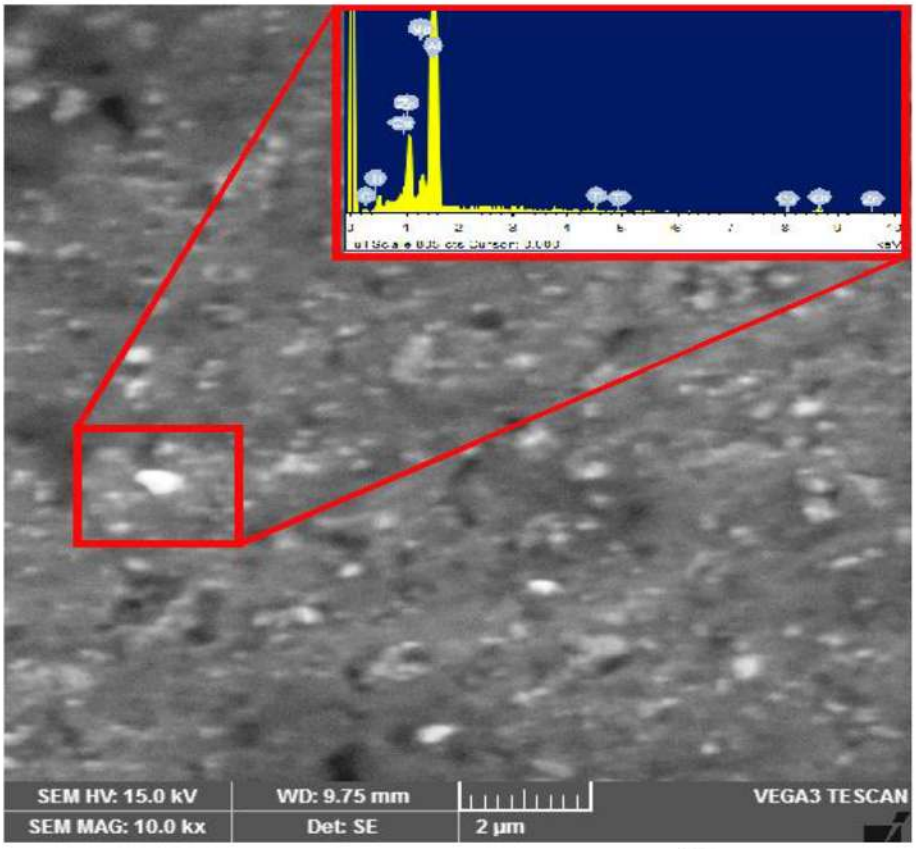

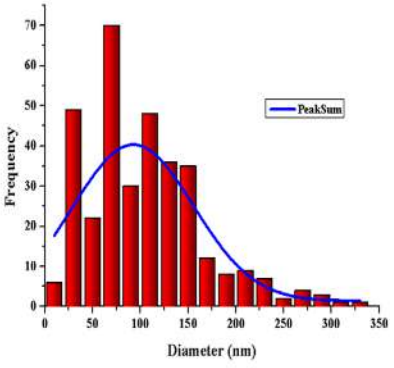

(B)

FIGURE 5 SEM photographs and comparable histogram of nanoparticles distribution of (A) AA7150-0.5 wt.% TiC (B) AA7150-1.0 wt.% TiC (C) AA7150-1.5 wt.% TiC (D) AA7150-2.0 wt.% TiC

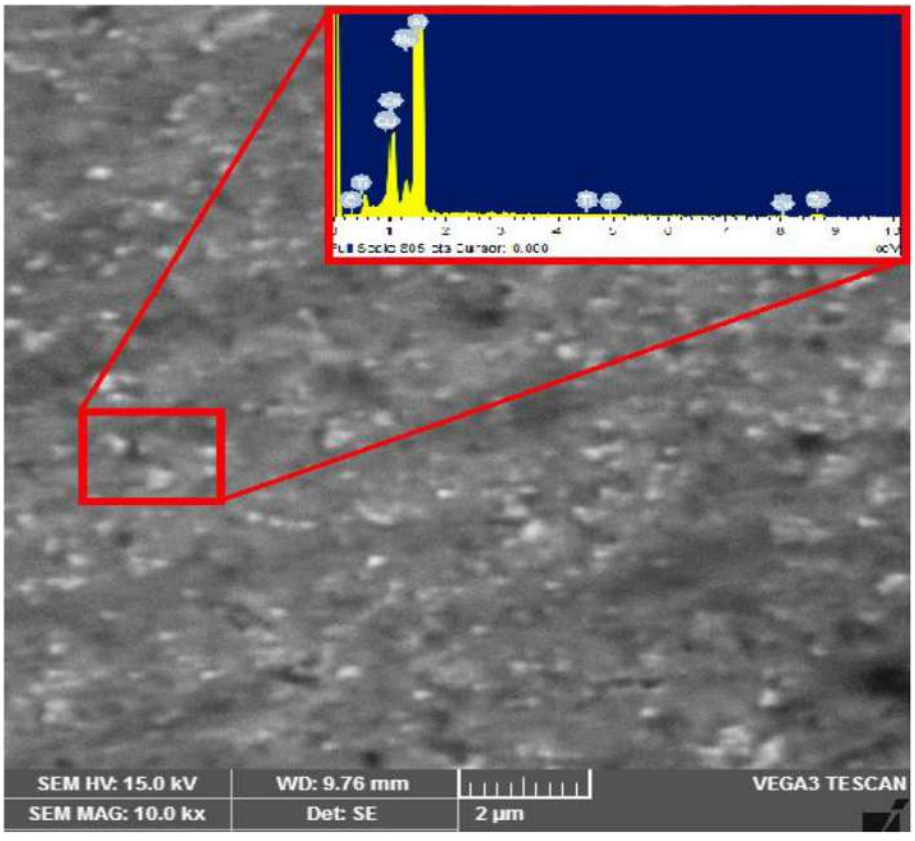

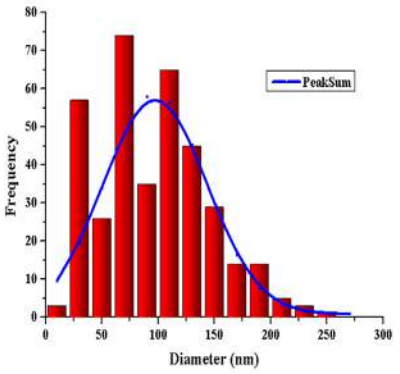

(C)

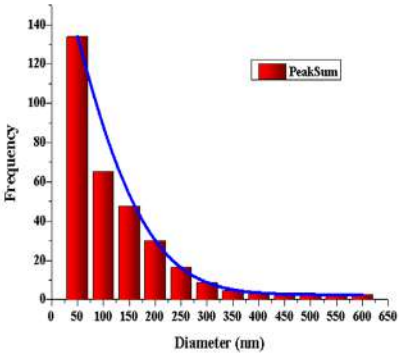

(D)

FIGURE 5 Continued

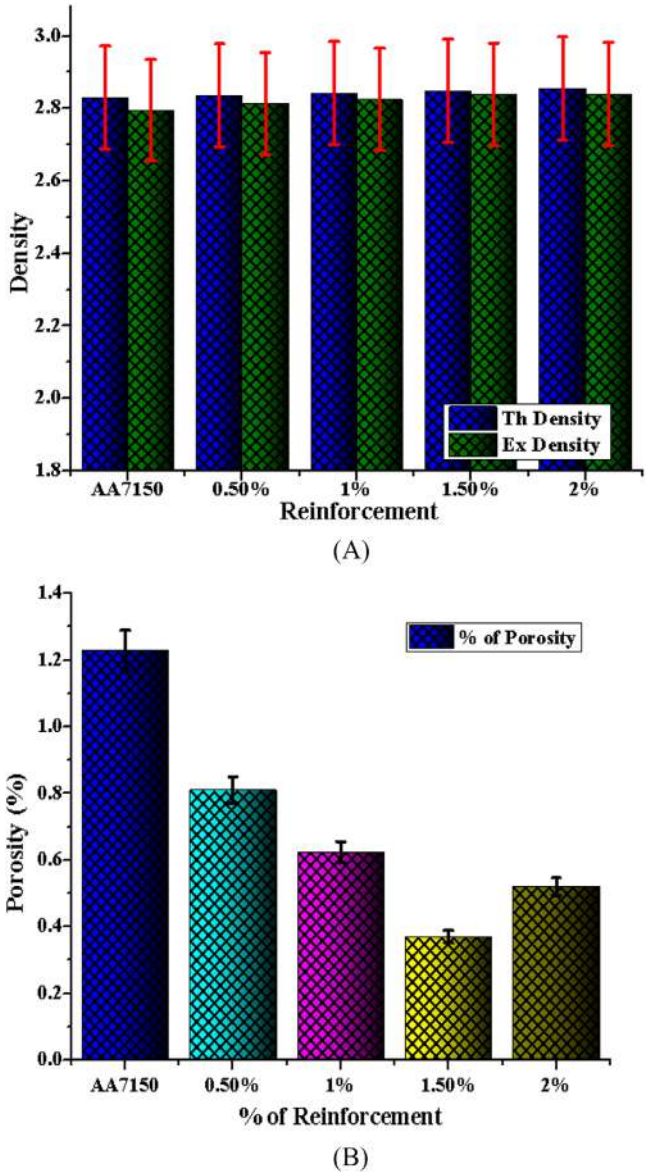

FIGURE 6 Influence of TiC percentage reinforcement on (A) Experimental and theoretical densities (B) Percentage of porosity

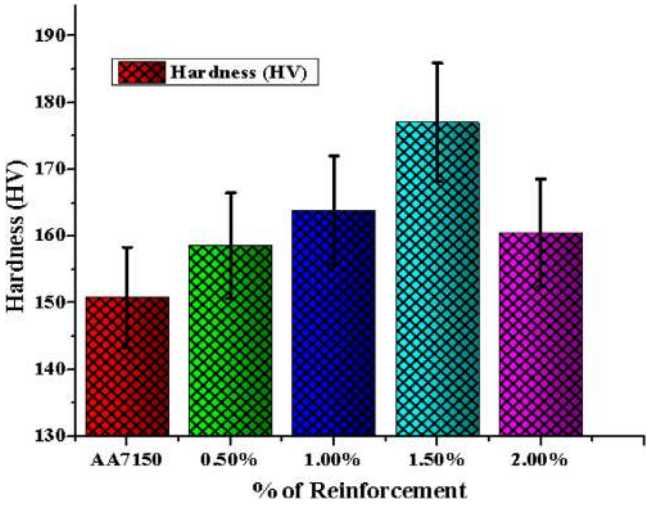

FIGURE 7 Effect of reinforcement on material hardness

particle distribution. The reason for the increase in microhardness of AA7150-TiC nanocomposites can be rightly attributed to the presence of TiC nanoparticles which are harder than AA7150 alloy and they prevent the movement of dislocation which ultimately increases microhardness as well as strength of the composite. Another thing that also contributes to the increase in microhardness of the nanocomposite is the large "surface to volume ratio" of ceramic nanoparticles. This large surface area increased the particle to matrix interface area, which leads to an increase in the microhardness of the nanocomposites.

The reason for the decrease in hardness value at 2 wt.% TiC can be rightly attributed to the formation of agglomeration of nano reinforcement and increased porosity content due to low nanoparticles percolation threshold effect. It can be confirmed with Figures 4E and Figure 5D.

Ultimate tensile strength (UTS) was carried out on AA7150-TiC nanocomposite and the tests were done according to ASTM E8M standard. "Universal Testing Machine (UTM) (INSTRON – 10 KN Load cell)" was used to conduct the UTS experiments. The specimens were fixed between the fixed and moving cross-heads of the UTM. The strength of different specimens was evaluated at a crosshead speed of 0.5 mm min^{-1}. The standard dimensions of the sample are as shown in Figure 8.

The influence of TiC nanoparticles reinforcement on the tensile strength of AA7150-TiC nanocomposites was analyzed through tensile test results and the graphical representation is as shown in Figure 9 and it was compared with monolithic material. The stress-strain graph showed the fracture surface of each AA7150-TiC based composite respectively. It is realized that the UTS values of TiC nanoparticulates reinforced composites are higher than the unreinforced matrix alloy. It is noticed that that the material strength enhanced with the increase in ceramic content. However, significant enhancement in strength is noticed when 1.5 wt.% TiC nanoparticle reinforcements were added. This is due to fact that porosity was estimated by ultrasonic degassing effects and the Hall-Petch grain refinement (strengthening) mechanism.[37] The grains were refined and equated to AA7150 matrix grains which promote the enhancement of UTS of AA7150-TiC nanocomposites. Moreover, it is a known fact that the Orowan strengthening mechanism is substantial while the size of the particle reinforcements is < 1 μm and when there is homogeneous dispersion throughout the alloy matrix.

The average particle size of TiC was 30–50 nm and these nanoparticles contribute to dislocation moment which leads to enhancement in the ultimate strength of

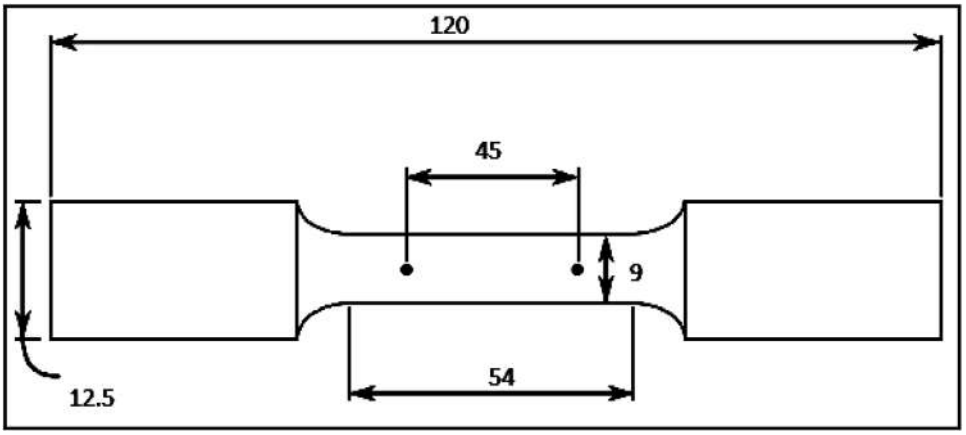

FIGURE 8 Tensile test specimen dimensions as per ASTM standards

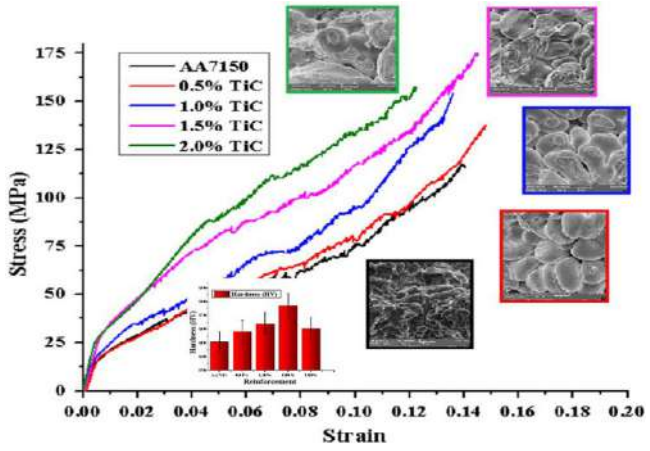

FIGURE 9 Stress-Strain curves, fracture surface (inset) and Vickers hardness (inset) of unreinforced and reinforced nanocomposites at room temperature

nanocomposites. The influence of the load sharing effect is minimal and the improvement of UTS is primarily due to grain refinement according to "Hall-Petch theory". The 1.5 wt.% TiC showed superior tensile strength value as compared to monolithic and other counterparts of the composites. The reason for the improvement in tensile strength (175 MPa) can be attributed to the uniform distribution of TiC nanoparticles which acts as a barrier to dislocation movement.

Under externally applied load, alloy matrix distributes the load to the ceramic particle reinforcement when there is solid interfacial bonding strength between two material phases.[38] This strengthening is attained by the distribution of reinforcement particle strengthening, dislocation and grain refinement strengthening.[39,40] The homogeneous dispersion of the TiC nanoparticles in matrix material provides marked improvement of distribution strengthening in AA7150-TiC nanocomposites through accommodating most of the applied forces which leads to improvement in load-bearing capacity of matrix alloy to ceramic particles. There is a decrease in tensile strength value for 2 wt.% TiC (158 MPa). The reason can be attributed to the formation of porosity and increased agglomeration of particles due to the limit on the threshold value of larger surface to volume ratio in the molten liquid.

The fracture surface of AA7150 alloy was observed at 100X magnification. Figure 10A shows the elliptical-shaped molecules of matrix alloy that are visible at 1000X magnification and it is also observed that the fracture is ductile in nature due to shearing effects and it is in turn brittle in nature while adding TiC nanoparticles content. Increasing TiC wt.% reduces the voids and elastic deformation due to the ultrasonication effect in the metal pool. This deformation can be observed along the fracture surface of the TiC reinforced composites.

Higher TiC nanoparticle reinforcement, the micro cracks are observed due to the cluster or agglomeration (supported by Figure 5D) which initiate and propagate the crack for the continuous loading and the surface shows the brittle fracture mode of Figure 10E. It is also due to the strong interface between the matrix alloy and TiC nanoparticles. Therefore, the failure of AA7150-TiC nanocomposite is a mixed-mode with partially ductile and partially brittle in nature.

4 | CONCLUSIONS

The novel fabrication method was successfully used to fabricate nanocomposites by enhancing the distribution of TiC nanoparticles in AA7150 based alloy. The material properties were increased with increased TiC nanoparticle reinforcement of upto 1.5% due to the sonication effect and then decreased due to clusters or agglomerations. Based on optical and SEM analysis, the grain size refinement and homogeneous distribution of TiC nanoparticles

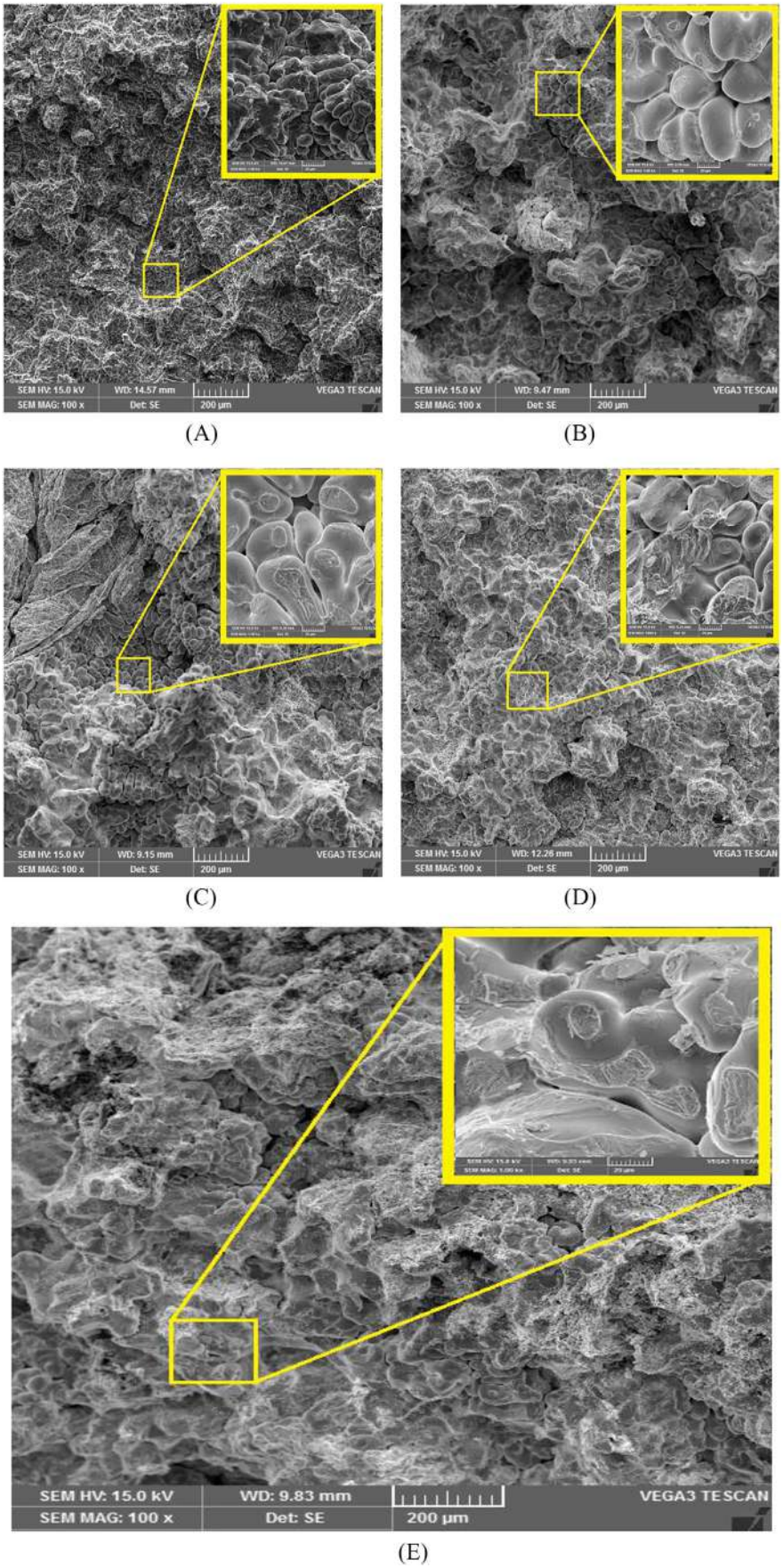

FIGURE 10 SEM photographs for fracture surface of (A) AA7150 (B) AA7150-0.5 wt.% TiC (C) AA7150-1.0 wt.% TiC (D) AA7150-1.5 wt.% TiC (E) AA7150-2.0 wt.% TiC

in AA7150-TiC nanocomposite were obtained due to the ultrasonic effect. The maximum grain refinement of the nanocomposite is 41.07 μm and the minimum porosity is 0.37% which were decreased by 52.37% (86.23-41.07 μm) and 69.87% (1.23-0.37%) as compared to AA7150 matrix alloy material. The microhardness and tensile strength of AA7150-TiC nanocomposites at as-cast case enhanced due to novel fabrication process followed by UV treatment effect. These properties of nanocomposites are 177.05 HV and 175 MPa, which are enhanced by 17.40% (150.81-177.05 HV) and 48.31% (118-175 MPa) as compared to the AA7150 alloy matrix, respectively.

ACKNOWLEDGMENTS

Author PM dedicates this research work to my beloved supervisor Prof. C. S. P. Rao, The Director of the National Institute of Technology-Andhra Pradesh (NIT-AP), India for his continuous support in my research work. Also, would like to that Dr. M. Raja Vishwanathan, Head, Humanities & Social Science Department, National Institute of Technology, Warangal (NIT-W), India for his valuable time spent proofreading the manuscript while giving useful suggestions. The KSU author is grateful to the Deanship of Scientific Research, King Saud University for funding through Vice Deanship of Scientific Research Chairs.

DATA AVAILABILITY STATEMENT

Research data are not shared.

ORCID

Murthy Chavali https://orcid.org/0000-0003-3910-2322

REFERENCES

1. B. R. Thella, *J. Tribol.* **2017**, *140*, 031601.
2. M. A. Salem, I. G. El-Batanony, M. Ghanem, *J. Eng. Mater. Technol.* **2017**, *139*, 011007.
3. R. Raj, D. G. Thakur. *Materialwissenschaft und Werkstofftechnik* **2018**, *49*, 1068.
4. P. Madhukar, N. Selvaraj, C. S. P. Rao, G. B. Veeresh Kumar. *Composites Part B* **2019**, *175*, 107136.
5. M. Rosa. Surface reinforcement of light alloys, surface modification by solid-state processing. Thesis, University of Lisbon **2014**, Ch. 4, p. 113.
6. S. Naher, D. Brabazon, L. Looney, *J. Mater. Process. Technol.* **2015**, *166*, 430.
7. S. A. Sajjadi, M. T. Parizi, H. R. Ezatpour, A. Sedghi, *J. Alloys Compd.* **2011**, *511*, 226.
8. M. Gupta, M. O. Lai, C. Y. H. Lim, *J. Mater. Process. Technol.* **2006**, *176*, 191.
9. B. Nili, G. Subhash, T. S. Tulenko. *ASME J. Manuf. Sci. Eng.* **2018**, *140*, 051010.
10. A. Ahmed, A. J. Neely, K. Shankar, P. Nolan, S. Moricca, E T. Synthesis, *Metall. Mater. Trans. A* **2010**, *41*, 1582.
11. J. Wang, D. Yi, X. Su, F. Yin, H. Li. *Mater. Des.* **2009**, *30*, 78.
12. Z. Xiu, W. Yang, G. Chen, L. Jiang, K. Ma, G. Wu. *Mater. Des.* **2012**, *33*, 350.
13. M. Kok, *J. Mater. Process. Technol.* **2005**, *161*, 381.
14. L. Liu, Y. Sheng, M. Liu, M. Dienwiebel, Z. Zhang, D. Dastan. *Tribo Int.* **2019**, *140*, 105727.
15. L. Sun, L. Liang, Z. Shi, H. Wang, P. Xie, D. Dastan, K. Sun, R. Fan. *Engine Sci.* **2020**, *12*, 95.
16. D. Roshita, D. Rupa, K. Prasad B. *ASME J. Tribol.* **2019**, *141*, 021605.
17. Z. Zhiyong, W. Yanli, X. Xiangjun, L. Yongfeng, Z. Laiqi, L. Junpin. *Adv. Eng. Mater.* **2015**, *17*, 1414.
18. J. Hashim, L. Looney, M. S. J. Hashmi, *J. Mater. Process. Technol.* **2002**, *123*, 251.
19. J. Hashim, L. Looney, M. S. J. Hashmi, *J. Mater. Process. Technol.* **2002**, *123*, 258.
20. M. A. Taha, N. A. El-Mahallawy, A. M. El-Sabbagh. *Adv. Eng. Mater.* **2003**, *11*, 805.
21. P. Madhukar, N. Selvaraj, C. S. P. Rao. *Mater. Sci. Eng.* **2016**, *149*, 12114.
22. S. Santanu, K. K. Santanu, D. Debdulal. *ASME J. Tribol.* **2019**, *141*, 041602.
23. H. Su, W. Gao, H. Zhang, H. Liu, J. Lu, Z. Lu. *ASME J. Manuf. Sci. Eng.* **2010**, *132*, 061007.
24. Y. Yong, L. Xiaochun, *J. Manuf. Sci. Eng.* **2007**, *129*, 497.
25. G. Cao, H. Konishi, X. Li. *Int. J. Metalcast.* **2008**, *2*, 57.
26. P. Madhukar, N. Selvaraj, G. Raghavendra, C. S. P. Rao. *Ultrason. Sonochem.* **2019**, *58*, 104665.
27. X. J. Wang, N. Z. Wang, L. Y. Wang, X. S. Hu, K. Wu, Y. Q. Wang, Y. D. Huang. *Mater. Des.* **2014**, *57*, 638.
28. X. Liu, S. Jia, L. Nastac. *Int. Metalcast.* **2014**, *8*, 51.
29. D. Dastan, A. Banpurkar, *J. Mater. Sci.: Mater. Electron.* **2017**, *28*, 3851.
30. P. Madhukar, Selvaraj N, G. B. Veeresh Kumar, C. S. P. Rao. *Ceramic Int.* **2020**, *46*, 17103.
31. K. Shan, Z. Z. Yi, X. T. Yin, L. Cui, D. Dastan, H. Garmestani, F. M. Alamgir, *J. Alloy Compd.* **2021**, *855*, 157465.
32. M. Pagidi, S. N, B. Veeresh Kumar G, P. Rao C S, M. Faruq, C. Murthy. *Mater. Sci. Eng.: B* **2021**, *265*, 115034.
33. N. Nishino, H. Kawahara, Y. Shimizu, H. Iwahori. *Grain Refinement of Magnesium Casting Alloys by Boron Addition*. WILEY-VCH, Weinheim **2000**, Ch. 10, p. 59.
34. K. V. Vinod, S. S. Meti, N. Jayakrishnan, K. R. Ravi, I. G. Siddhalingeshwar. *Trans. Indian Inst. Met.* **2018**, *71*, 841.
35. J. Li, T. Momono, Y. Tayu, Y. Fu. *Mater. Lett.* **2018**, *62*, 4152.
36. J. W. Li, T. Momono, Y. Tayu. *Mining Metallurg Eng.* **2007**, *2*, 13.
37. R. Harichandran, N. Selvakumarg. *Int. J. Mech. Sci.* **2017**, *144*, 814.
38. R. R. Chen, D. S. Zheng, T. F. Ma, H. S. Ding, Y. Q. Su, J. J. Guo, H. Z. Fu. *Ultrason. Sonochem.* **2017**, *38*, 120.
39. K. Narendra, G. Gaurav, K. G. Rakesh, M. Anita, M. Sunil, *J. Eng. Mater. Technol.* **2017**, *139*, 011002.
40. B. Mohan, A. M. Thirumal, A. Rajadurai. *ASME Proc.* **2015**, *IMECE2015-53151*, V02BT02A062.

How to cite this article: P. Madhukar, N. Selvaraj, G. B. V. Kumar, C. S. P. Rao, F. Mohammad, R. Seetharam, M. Chavali, *Nano Select* **2021**, 1. https://doi.org/10.1002/nano.202100094